BASIC RESEARCH www.jasn.org

Quantitative Three-Dimensional Tissue Cytometry to Study Kidney Tissue and Resident Immune Cells

Seth Winfree,* Shehnaz Khan,* Radmila Micanovic,* Michael T. Eadon,* Katherine J. Kelly,* Timothy A. Sutton,* Carrie L. Phillips,† Kenneth W. Dunn,* and Tarek M. El-Achkar*‡

*Division of Nephrology, Department of Medicine and †Department of Pathology, Indiana University School of Medicine, Indianapolis, Indiana; and ‡Department of Medicine, Roudebush Veterans Affairs Medical Center, Indianapolis, Indiana

ABSTRACT

Analysis of the immune system in the kidney relies predominantly on flow cytometry. Although powerful, the process of tissue homogenization necessary for flow cytometry analysis introduces bias and results in the loss of morphologic landmarks needed to determine the spatial distribution of immune cells. An ideal approach would support three-dimensional (3D) tissue cytometry: an automated quantitation of immune cells and associated spatial parameters in 3D image volumes collected from intact kidney tissue. However, widespread application of this approach is limited by the lack of accessible software tools for digital analysis of large 3D microscopy data. Here, we describe Volumetric Tissue Exploration and Analysis (VTEA) image analysis software designed for efficient exploration and quantitative analysis of large, complex 3D microscopy datasets. In analyses of images collected from fixed kidney tissue, VTEA replicated the results of flow cytometry while providing detailed analysis of the spatial distribution of immune cells in different regions of the kidney and in relation to specific renal structures. Unbiased exploration with VTEA enabled us to discover a population of tubular epithelial cells that expresses CD11C, a marker typically expressed on dendritic cells. Finally, we show the use of VTEA for large-scale quantitation of immune cells in entire human kidney biopsies. In summary, we show that VTEA is a simple and effective tool that supports unique digital interrogation and analysis of kidney tissue from animal models or biobanked human kidney biopsies. We have made VTEA freely available to interested investigators *via* electronic download.

J Am Soc Nephrol 28: ●●●–●●●, 2017. doi: 10.1681/ASN.2016091027

Resident immune cells are among the most specialized cells in the renal interstitium. These cells play a critical role in defense against foreign pathogens. However, resident immune cells are also responsible for regulating key homeostatic functions, independent of pathogen interactions. The importance of this local immune network in kidney health and disease has become increasingly recognized.[1,2]

An essential step in characterizing a local immune response is the identification of the specific immune cell subtypes that are involved.[1–3] In fluid specimens, these identifications are typically accomplished using flow cytometry (FC). FC can also be used to characterize immune cells in homogenized solid organs, such as the kidney.[4–10] However, when cells are isolated from the kidney for such analysis, they are isolated by enzymatic digestion, destroying all spatial information potentially critical to understanding the function of the renal resident immune cells. Furthermore, the application of FC to the study of human specimens is limited by the small amounts of tissue collected.

Given the essential similarity between FC and laser-scanning microscopy, an obvious solution would be to conduct cytometry-like analyses of three-dimensional (3D) images collected from intact

Received September 23, 2016. Accepted December 29, 2016.

Published online ahead of print. Publication date available at www.jasn.org.

Correspondence: Dr. Tarek M. El-Achkar or Dr. Kenneth W. Dunn, 950 West Walnut, R2 E224, Indiana University School of Medicine, Division of Nephrology, Indianapolis, IN 46202. Email: telachka@iu.edu or kwdunn@iu.edu

kidney tissue. Modern optical sectioning microscopy, such as confocal and light sheet microscopy, allow for the collection of large 3D datasets.[11] These types of datasets have the potential to support quantitative surveys of various cell types within the spatially preserved context of the intact tissue, a process that we refer to as 3D tissue cytometry. Compelling demonstrations of the value of this approach were shown in the works by Gerner *et al.*[12] and Moreau *et al.*,[13] which used 3D tissue cytometry to discriminate and localize several immune cell populations in mouse tissue, and the work by Liarski *et al.*,[14] which used tissue cytometry to measure distances between lymphocytes in human kidney biopsies.

Although the capability to perform 3D imaging of kidney tissue is widely available, a rate-limiting step in the analysis of image volumes from such a large and complex organ lies in the lack of accessible image processing tools designed to support efficient exploration and quantitative analysis of large 3D image volumes. The quantitative analyses described above were based upon a complex pipeline of sophisticated image processing methods applied through multiple custom-designed or commercial software packages. Here, we describe software that we developed that combines the different image processing and analysis components of 3D tissue cytometry into a single integrated workspace that is both powerful and user friendly. Volumetric Tissue Exploration and Analysis (VTEA) software is designed for efficient exploration and quantitative analysis of large, complex 3D microscopy datasets using the tools and interface of ImageJ. We show the utility of VTEA in analyses of the resident immune system in intact, fixed kidney tissues. We show that VTEA can be used to measure the abundance and spatial distribution of distinct types of epithelial and immune cells within a volume of imaged kidney tissue. Taking advantage of the preserved morphologic landmarks, we also show that VTEA can be applied in a high-resolution discovery mode to identify previously unrecognized subtle but potentially important findings, such as the discovery of distinct subtypes of tubular epithelial cells or regional clustering of antigen-presenting cells. Finally, we show how VTEA can be applied for large-scale analysis of whole-core human kidney biopsies, which could extend its use to investigate human kidney disease.

RESULTS

3D tissue cytometry depends on spatially distinguishing individual cells in fixed kidney tissue after fluorescent labeling and volumetric imaging. We have taken the approach of identifying individual cells by their nuclei using the fluorescent DNA-binding probe 4′,6-diamino-2-phenylindole (DAPI), which labels all nucleated cells. DAPI-labeled nuclei are highly amenable to automated segmentation, because they are brightly fluorescent, spatially distinct, and relatively uniform in size and shape.[15] To identify different types of cells, tissues are incubated with antibodies to proteins characteristic of different cell types, and cells are classified on the basis of the levels of immunofluorescence measured within a defined 3D distance of the nucleus. The overall VTEA workflow, consisting of nuclear segmentation, cellular quantification, and data analysis, is depicted schematically in Figure 1 and Supplemental Figure 1, which show various windows from the integrated VTEA graphic user interface. Below, the details and special features of this workflow are described at length with specific examples.

Identification and Quantitation of Renal Tubular Cells in Kidney Sections

To show the utility of VTEA, we first explored its application in identifying and measuring the density of specific tubular cell types in approximately $600\times600\times50$-μm^3 image volumes of a human nephrectomized kidney (Figure 2). Cortical kidney sections were imaged with 3D confocal microscopy after staining with DAPI (to label nuclei), Oregon Green Phalloidin (to label filamentous actin [F-actin]), and an antibody to aquaporin-2 (AQP2; to label collecting duct). 3D renderings of the resulting volume are shown in Figure 2A, which shows the characteristically strong actin labeling of the vasculature and brush border of the proximal tubule (Figure 2A, cyan) and bright AQP2 immunofluorescence of principal cells in collecting ducts (Figure 2A, yellow). The VTEA software was used to segment individual nuclei for the entire volume (shown in white in Figure 2A) in 3D, measure DAPI fluorescence and AQP2 immunofluorescence for each nucleus, and display the resulting measurements in the form of a scatterplot, similar to how FC results are typically displayed and evaluated (Figure 2B).

In the example shown, a total of 2411 cells were identified. As with the FlowJo software (FlowJo, LLC, Ashland, OR) used to analyze FC data, VTEA supports drawing regions of interest (ROIs; or gates) on the scatterplots, which can be used to select groups of cells with particular quantitative features. Using this approach, VTEA identified 229 (9.5% of total) cells as positive for AQP2. A unique and powerful feature of VTEA is that the nuclei of cells gated on the scatterplot are immediately highlighted on the original image, supporting interactive exploration of the localization of cells identified on the scatterplot. As expected, the gate isolating cells high in AQP2 immunofluorescence identifies a set of tubular cells distributed in a cobblestone pattern characteristic of principal cells of the collecting duct (Figure 2B; red arrowheads and red overlay in Figure 2C). We also observed a small number of these AQP2+ cells in other tubules (white arrowheads in Figure 2C), most likely identifying connecting segments.

Another unique feature of VTEA is that it supports quantitative analysis of cells located in ROIs drawn by the user on the image volume. Figure 2D shows how this feature was used to characterize cells associated with the collecting duct. We drew an ROI on the original volume to isolate a single tubule and used VTEA to measure the fraction of AQP2+ cells within the ROI (Figure 2D). Analysis of the cells located in the ROI showed that 82% of the cells gated for high levels of AQP2 are found in the tubule demarcated by the ROI (Figure 2E).

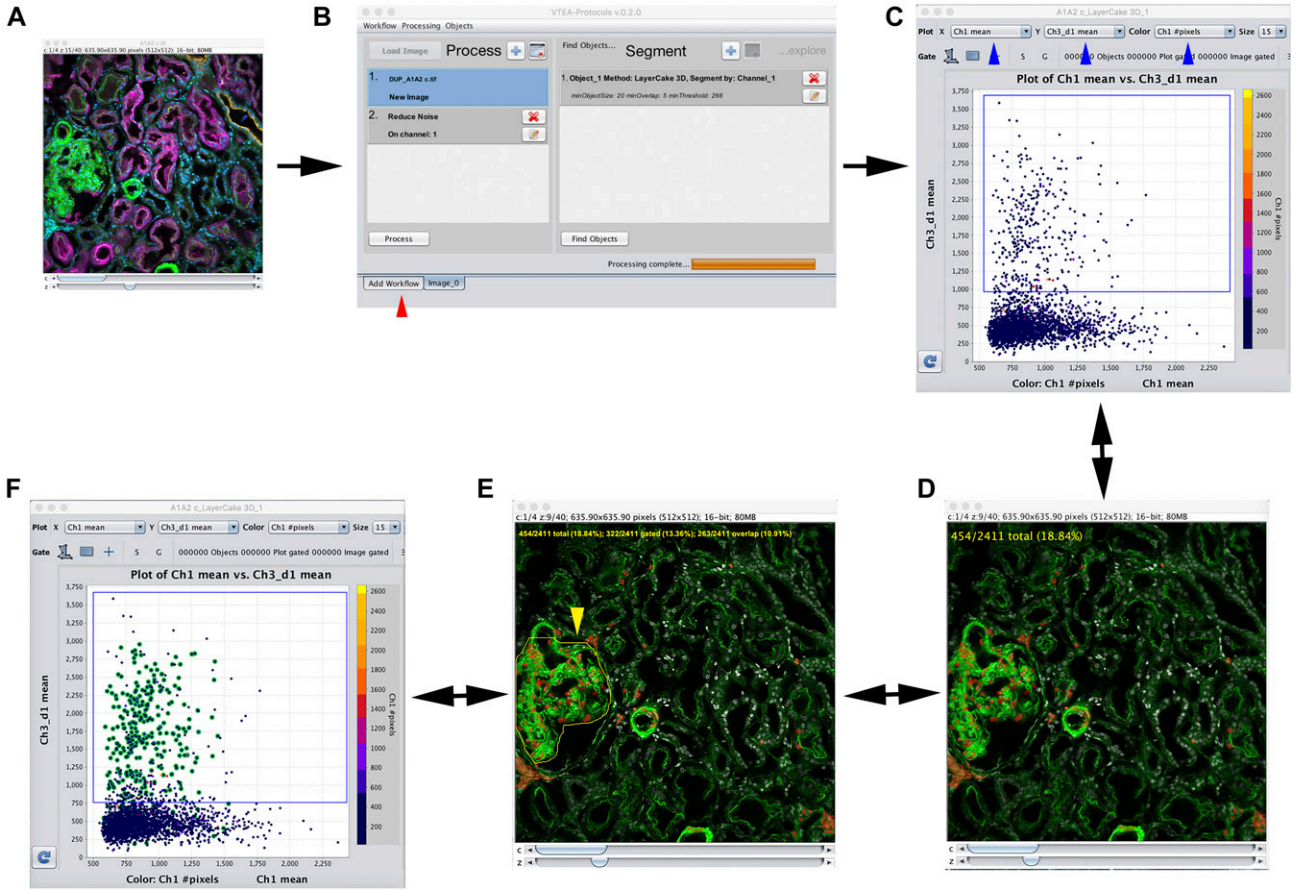

Figure 1. Demonstration of tissue cytometry workflow using VTEA plugin for ImageJ. VTEA plugin for 3D tissue cytometry organizes image processing, cell identification, and interactive exploration of cell populations. (A) A four-channel image volume loaded into ImageJ/FIJI. (B) Basic image preprocessing (*e.g.*, background subtraction and noise reduction) and 3D segmentation (using one of several algorithms) are controlled through the VTEA plugin GUI. Multiple datasets can be analyzed simultaneously and in parallel *via* a tabbed interface as indicated by the red arrow. (C) Segmented 3D objects (in this case, nuclei) are quantified by clicking the Find Objects button, which generates a scatterplot GUI, in which each dot represents measured parameters for a single cell. Up to three measurement parameters (*e.g.*, intensities, morphology) can be selected for simultaneous display (*x* axis, *y* axis, and color) *via* a menu interface (blue arrows). (D) Rectangles can be drawn on the scatterplot to identify subpopulations of cells (gating), which are highlighted in user-defined colors in the image volume to identify their spatial distribution (shown here in red). Alternatively, (E) free-hand ROIs can be drawn on the image volume to isolate particular structures (in this case, a yellow region is drawn around a glomerulus), which (F) generates a new scatterplot displaying quantifications for cells from the demarcated region (shown here as green-outlined dots).

Therefore, by using image ROIs, VTEA can be used to directly quantify the number of cells associated with structures visualized on image volumes. We emphasize that VTEA analyses are all conducted in 3D, increasing the number of cells in the census and avoiding artifacts resulting from the limited scope of single optical sections (Supplemental Figures 2 and 3, Supplemental Movie 1).

VTEA of Resident Mononuclear Phagocytic Cells in the Kidney

We next tested the capability of VTEA for investigating the distribution of mononuclear phagocytic cells (MPCs) in mouse kidney tissue. We labeled mouse kidney tissue with DAPI, fluorescent phalloidin, and antibodies to MHCII and CD11C, cell surface proteins specific to MPCs. Confocal microscopy was used to collect a 3D image volume from a $600\times600\times50$-μm^3 region of the tissue. A single plane of the resulting volume and a 3D rendering of the volume are shown in Figure 3A. We used VTEA to distinguish 3384 cells in the image volume; quantify DAPI, MHCII, and CD11C immunofluorescence for each cell; and identify MPCs by drawing gates identifying cells with high levels of MHCII and/or CD11C immunofluorescence (Figure 3, B and C). By plotting DAPI fluorescence intensity versus MHCII intensity and gating on the MHCII axis, we identified 142 MHCII+ cells, representing 4.2% of the cells in the image volume (gate 1 in Figure 3B). To identify MHCII+ cells lacking CD11C, we plotted CD11C versus MHCII intensity for each cell (Figure 3C). By applying

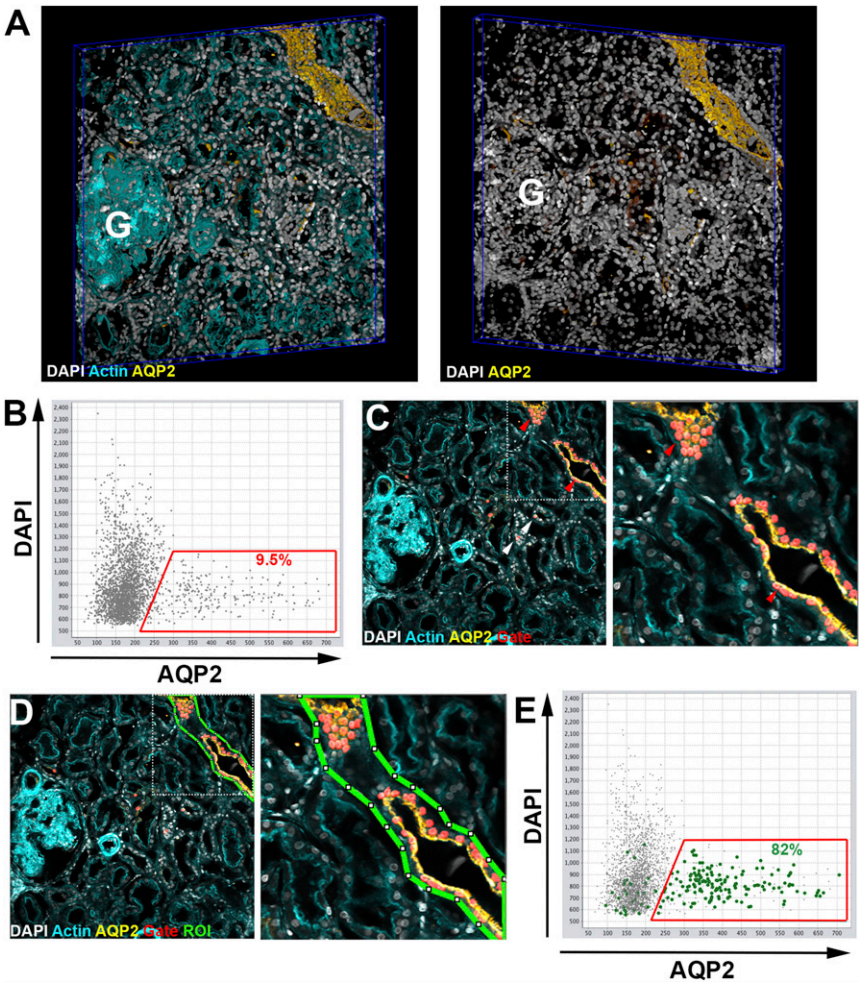

Figure 2. VTEA can discriminate renal tubular types on the basis of cellular markers. Sections from a human kidney nephrectomy were fixed and stained for nuclei (gray), F-actin (cyan), and AQP2 (yellow). (A) 3D rendering of an image volume with a glomerulus indicated (G). At left, a rendering of the nuclei and AQP2 is shown. (B) VTEA scatterplots with cell-associated AQP2 and DAPI intensities plotted on the *x* and *y* axes. (C) Mapping gated cells to the original image volume. The cells identified in B were mapped to the original image volume with a red overlay; a single plane is shown. AQP2+ principal cells of collecting ducts (CDs) and cells in connecting tubules are indicated by red and white arrowheads, respectively. Inset is taken from the indicated region in left panel. (D) Restricting VTEA to subvolumes with an ROI verifies AQP2+ cells in the CD. An ROI was drawn on a single slice as indicated in green. Inset given at right. (E) Mapping of cells back to the scatterplot. Cells selected by the ROI in D were highlighted in green on the original scatterplot from B. The percentage of cells identified is indicated.

a gate for cells high in MHCII but low in CD11C fluorescence intensity, we determined that 100 of the MHCII+ cells in the image volume (70%) lack CD11C (gate 3). This example shows VTEA's ability to efficiently survey and analyze large numbers of cells in tissue samples, providing investigators with a uniquely powerful tool for tissue interrogation.

In many cases, discriminating a particular population of cells requires simultaneous consideration of more than two parameters. To accommodate three parameters on a conventional two-dimensional (2D) scatterplot, VTEA offers the ability to display the points of the scatterplot in colors corresponding to measured values. For instance, we expect that cells lining the vasculature will be rich in F-actin but will lack MPC markers MHCII and CD11C. In Figure 3C, we have displayed the mean intensity of the measured actin fluorescence in color to simultaneously compare levels of actin, MHCII, and CD11C. As expected, higher levels of actin fluorescence are detected only in cells lacking MHCII and CD11C (Figure 3C, red through yellow points), consistent with the general absence of these antigens from endothelial cells and/or smooth muscle cells of the vasculature.

We then used VTEA's unique ability to display gated cells in the original image volume to evaluate the spatial distribution of different MPCs. Nuclei of cells gated for high levels of MHCII in the scatterplot shown in Figure 3B are indicated in yellow in the volume renderings shown below the scatterplot.

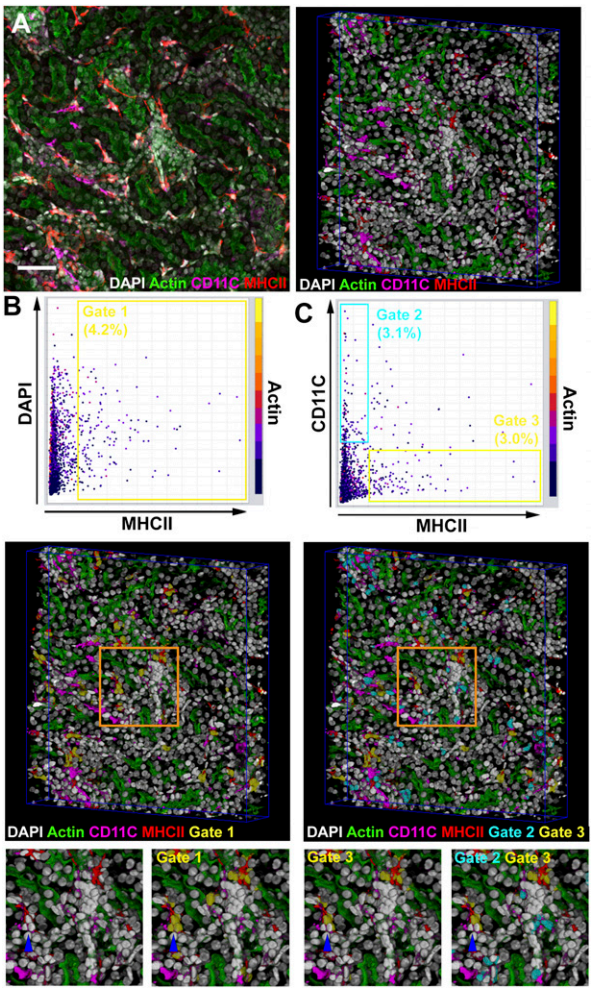

Figure 3. VTEA allows for precise quantitation of renal MPCs. Whole mouse kidneys were fixed, sectioned, and stained for nuclei (gray), F-actin (green), MHCII (red), and CD11C (magenta). (A) A maximum intensity projection and 3D rendering of an image volume from the cortex illustrates the morphologic complexity and the large number of cells. (B) Cells were identified in the volume from A, and their average DAPI versus the average MHCII intensity was plotted. A gate was drawn identifying 142 cells with high MHCII immunofluorescence. These gated cells are highlighted in yellow in the rendered volume and magnified regions shown below B. (C) An additional marker for MPCs defines a second distinct population of interstitial cells. The average intensities of CD11C and MHCII immunofluorescence were plotted, and two separate gates were drawn to identify CD11C+/MHCII− cells (gate 2) or CD11C−/MHCII+ cells (gate 3). These gated cells are highlighted in cyan and yellow, respectively, in the rendered volume and magnified regions shown below C. Blue arrowheads indicate cell selectivity in gates from B and C.

Nuclei of cells gated as MHCII+/CD11C− or MHCII−/CD11C+ in the scatterplot of Figure 3C are depicted in yellow and teal, respectively, in the volume renderings shown below the scatterplot. The ability to highlight gated cells on the image volume thus enables VTEA to display the 3D distribution of immune cell subtypes relative to each other.

We next used VTEA to measure the abundance and distribution of MHCII and CD11C MPCs in different regions of the kidney. 3D image volumes of mouse kidney tissue labeled as described above were collected from either the cortex or the outer stripe. Using the techniques described above, VTEA was then used to process and quantify the resulting image volumes and generate scatterplots comparing the levels of CD11C and MHCII immunofluorescence in the cortex and outer stripe (Figure 4A). MPCs identified on the scatterplots were gated into three populations: CD11C+/MHCII− cells (gate a), CD11C+/MHCII+ cells (gate b), or CD11C−/MHCII+ cells (gate c). Quantitative VTEA analysis showed a distinct distribution of each type of MPC in different regions of the kidney (Figure 4C); MHCII+ CD11C− MPCs are significantly more abundant in the cortex, whereas MHCII− CD11C+ MPCs are significantly more abundant in the outer stripe (2.6%±0.14% versus 1.2%±0.3% and 1.7%±2.1% versus 8.8%±4.7%, respectively; $P<0.05$ for each; $n\geq3$ mice for each). In Figure 4D, these gated cells are highlighted in the original volume and indicate several clusters of MHCII− CD11C+ cells (Figure 4D, red nuclei), MHCII+ CD11C− cells (Figure 4D, magenta nuclei), and MHCII+ CD11C+ cells (Figure 4D, yellow nuclei). To refine the localization of the MHCII+ cells in microenvironments of the cortex, we used VTEA to test association of MHCII+ cells with different tubular subsegments and showed that MHCII+ cells are more abundant near glomeruli (Supplemental Figure 4). By quantifying the distribution of specific MPCs in different regions of the kidney and identifying associations with renal structures, these examples show how VTEA provides unique insights that suggest spatially specialized functions of MPCs in the kidney.

VTEA Extends Results Provided by FC

FC's rapid assessment of thousands of cells provides statistically relevant quantitation. Can VTEA generate similarly significant data while maintaining spatial information? To compare results obtained using VTEA with those obtained from FC, we used both techniques to analyze the effect of knocking out Tamm–Horsfall protein (THP) on the abundance of MHCII+ cells in the mouse kidney. FC of kidney lysates shows that the loss of THP results in an approximately 30% decrease in the percentage of MHCII+ cells (Figure 5A). Consistent results were obtained using VTEA, which additionally showed that the loss of MHCII+ cells was most pronounced in the inner stripe, where MHCII+ cells are most abundant (Figure 5B). This spatial information may be critical to understanding how the loss of THP influences MHCII+ cells. Given the abundance of THP in the inner stripe, the localized depletion of MHCII+ cells in the interstitium of the inner stripe suggests that THP may be needed for proper formation of the MPC network in the kidney and specifically, the inner stripe.

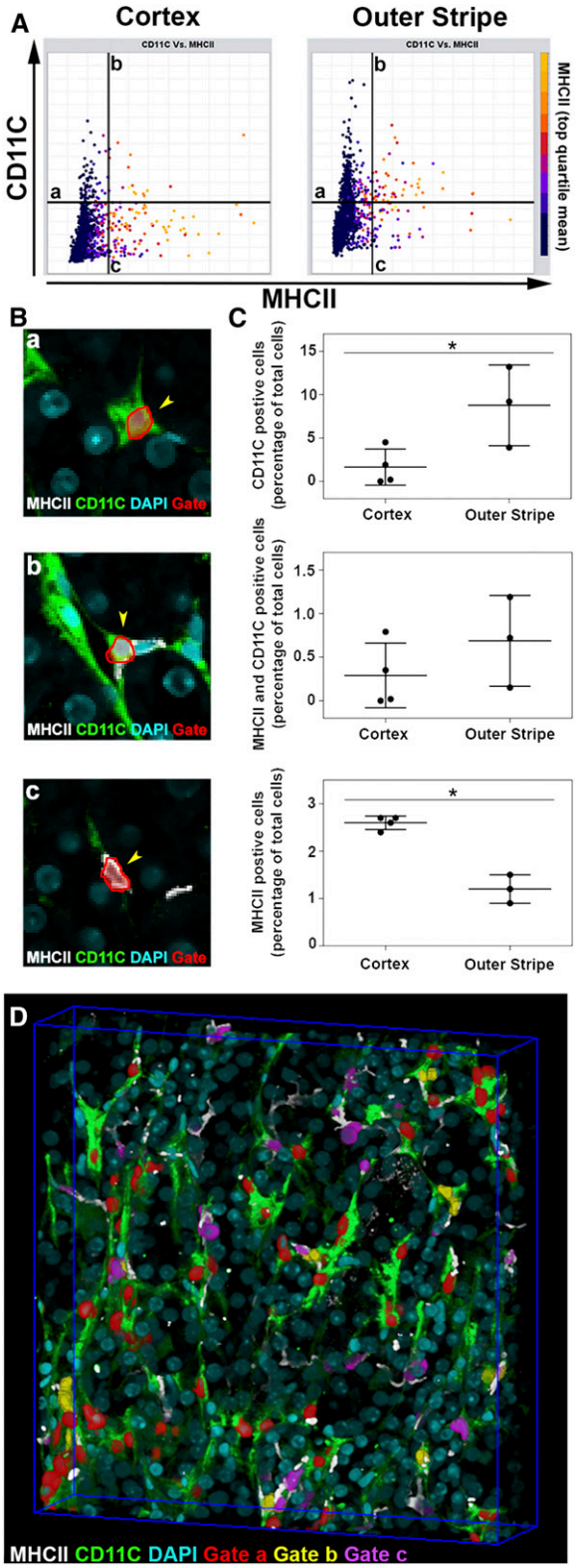

Figure 4. Quantitating the distribution of MPCs in different regions of the kidney using VTEA. Mouse kidney sections were fixed and stained for nuclei (cyan), MHCII (white), and CD11C (green) imaged by confocal microscopy and analyzed *via* VTEA. (A) Scatterplots showing CD11C versus MHCII immunofluorescence for samples collected from the cortex (left panel) and outer stripe (right panel). Gates were drawn to identify CD11C+/MHCII− cells (gate a), CD11C+/MHCII+ cells (gate b), or CD11C−/MHCII+ cells (gate c). (B) Examples of MPCs identified with gates a–c (highlighted and outlined in red and indicated with arrowheads). (C) Summary of results obtained from VTEA analysis comparing the relative abundance of CD11C+/MHCII− cells (gate a), CD11C+/MHCII+ cells (gate b), or CD11C−/MHCII+ cells (gate c) in the cortex and outer stripe. *$P<0.05$ for an unpaired *t* test ($n\geq3$ mice for each). (D) A 3D rendering of a volume collected from the outer stripe with red, yellow, and magenta overlays used to indicate cells localized by VTEA to gates a–c, respectively.

VTEA as a Tool for Discovery—Uncovering Rare Cell Subtypes

When stained with DAPI, the nuclei of interstitial cells are generally significantly brighter than the nuclei of tubular cells (cyan versus white arrowheads, respectively, in Figure 6B). Interestingly, when we used VTEA to gate a subpopulation of CD11C+ cells with low levels of DAPI fluorescence (gate 2 in Figure 6A) and map these cells into the original image volume (shown in yellow in Figure 6, C and D), we uncovered a population of proximal tubular cells expressing CD11C (yellow arrowheads in Figure 6C). Further analysis showed that these cells were more abundant in the outer stripe, localized to the S3 segments of proximal tubules (3.1%±0.73% versus 0.32%±0.44%, respectively; $P<0.05$) (Figure 6E). In the cortex, CD11C+ tubular cells were almost exclusively localized in S1 segments that are contiguous with Bowman's space (Supplemental Movie 2). The significance of these findings is still unclear, but this example shows how the bidirectional workflow of VTEA was used to detect what may be a specialized phenotype of a specific set of proximal epithelial cells.

Using VTEA for Large-Scale Analysis of Human Kidney Biopsy Cores

As shown above, VTEA is an efficient tool for analyzing high-resolution confocal image volumes. We next asked if we could apply this same level of analysis to large-scale analysis of sections from frozen human kidney biopsies. To this end, we imaged 50-μm-thick sections of kidney biopsy cores taken from two patients with diabetic nephropathy and stained for nuclei, F-actin, myeloperoxidase (a marker for neutrophils), and CD45R (a marker for B lymphocytes) (Figure 7A). We then used VTEA to analyze the entire approximately 4 mm ×0.5 mm ×50-μm^3 volumes and quantitatively determine the number and fraction of infiltrating neutrophils and B cells in both biopsies. This analysis identified noticeable differences between the two biopsies (Figure 7, B and C). In particular, neutrophils represented only 0.31% of the cells in the biopsy obtained from patient A but represented 2.04% of the cells in the biopsy obtained from patient B. Interestingly, these two patients also differed significantly with respect to the progression of kidney disease (Figure 7D). Although premature, this analysis shows the viability of tissue cytometry for the analysis of human kidney

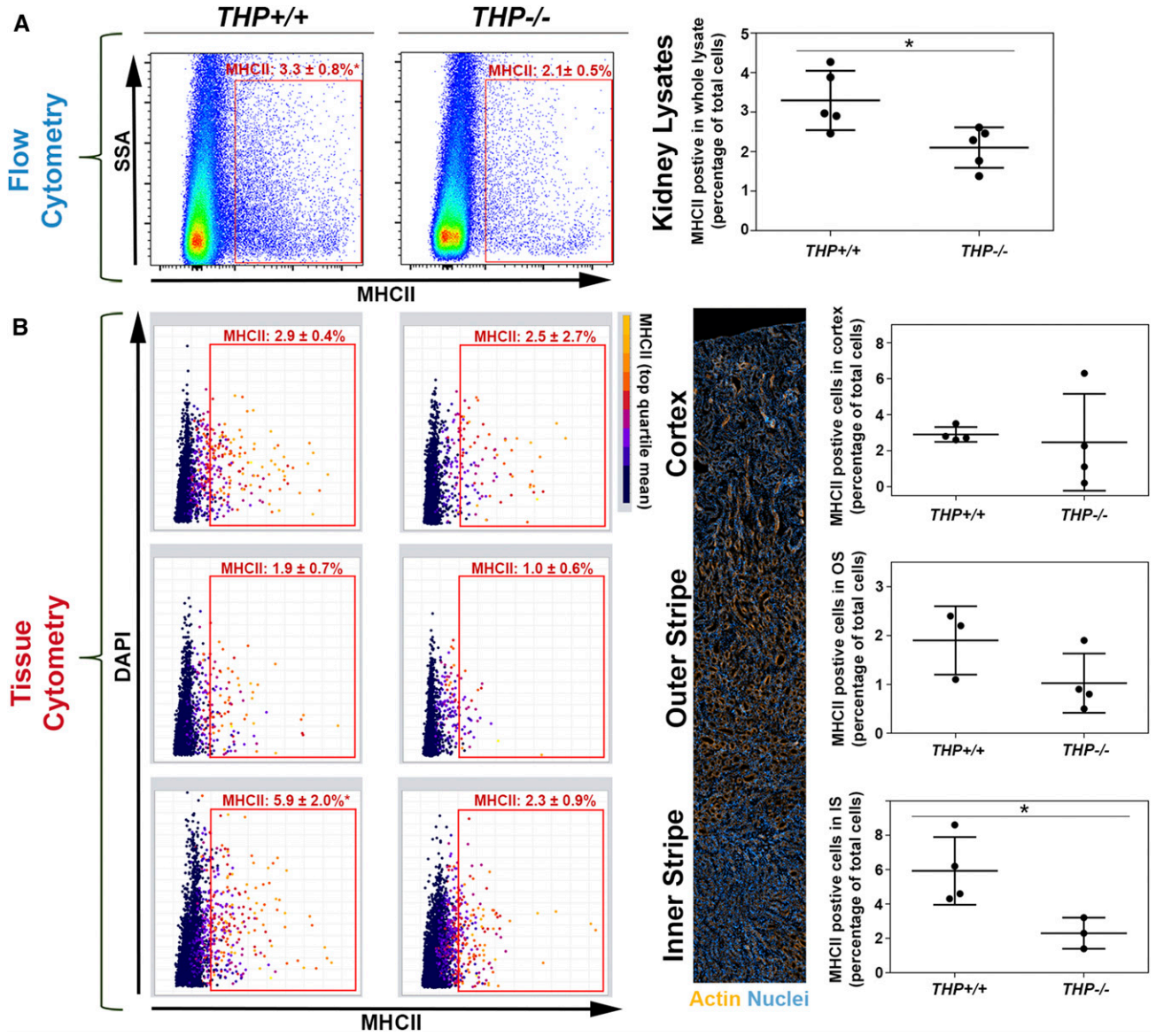

Figure 5. The spatial information provided by VTEA extends results provided by FC. Whole mouse kidneys from either a parental line (THP+/+) or THP−/− were homogenized and stained for MHCII or fixed, sectioned, and stained with DAPI and for MHCII. The whole-kidney lysates were then subjected to FC, and the kidney sections were imaged by confocal microscopy and subjected to VTEA analysis. (A) FC of whole-kidney lysates indicates the loss of MHCII+ cells in the kidney of mice lacking THP (3.3%±0.8% versus 2.1%±0.5%; $n \geq 3$ mice for each condition). (B) VTEA analysis of image volumes collected from the cortex (top panel), outer stripe (middle panel), and inner stripe (bottom panel). Representative scatterplots of MHCII versus DAPI are shown for volumes collected from each region. Mean percentages (±SD) represent analyses of at least three mice for each condition. Summary graphs (right panel) show that MHCII cells are primarily lost from the inner stripe of THP−/− mice.

biopsies and illustrates how VTEA-based tissue cytometry could be combined with other clinical data to provide unique insights into the pathogenesis of human kidney disease.

DISCUSSION

The size and intricacy of large-scale 3D image volumes collected from complex organs, such as the kidney, are incompatible with traditional histology approaches. 3D volumes cannot be evaluated by inspection of individual image planes, but must be viewed as 3D renderings. The quantitative analysis of thousands of cells arrayed in 3D cannot be accomplished manually but instead, requires automated methods of 3D image processing, segmentation, and quantification. Previous studies showing the power of quantitative 3D tissue cytometry for studies of the immune system depended on image analysis procedures conducted using combinations of commercial and custom

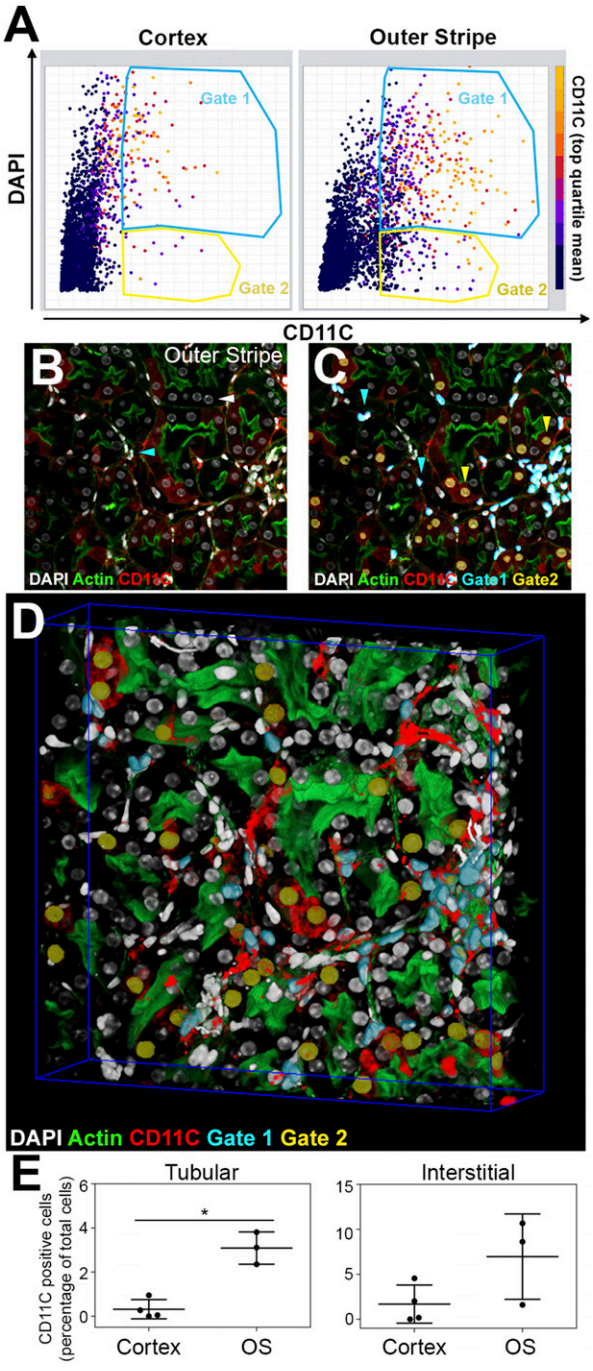

Figure 6. Using VTEA based analysis to uncover CD11C+ tubular epithelial cells. Mouse kidney sections were fixed and stained for nuclei (white), F-actin (green), and CD11C (red) imaged by confocal microscopy and analyzed *via* VTEA. (A) Scatterplots of CD11C versus DAPI fluorescence from samples collected from either the cortex or outer stripe of the kidney show that CD11C is present in cells with high or low levels of DAPI fluorescence. (B) An example of an image of a single focal plane collected from the outer stripe. (C) The same focal plane shown in B but with the nuclei of CD11C+ cells gated for high and low levels of DAPI highlighted in cyan and yellow, respectively. Surprisingly, this image clearly shows that most of CD11C+ cells with low levels of DAPI fluorescence are proximal tubular epithelial cells (adjacent to bright actin-labeled brush border). (D) A rendering of the entire 3D volume, with nuclei of CD11C+ cells gated for high and low levels of DAPI highlighted in cyan and yellow, respectively. (E) Quantitation of the abundance of high and low DAPI-gated cells in samples collected from the cortex or outer stripe shows that the low-DAPI cells, largely proximal tubule cells, are significantly more abundant in the outer stripe than in the cortex ($P<0.05$; $n\geq3$ mice for each).

software with cost and/or sophistication that are beyond the reach of many biomedical researchers. We developed VTEA in response to the need for an integrated, efficient, and simple digital image analysis solution for 3D tissue cytometry. The unique values of our integrated approach are that (*1*) it requires mastery of a single software system, (*2*) the component tools are organized into an intuitive image analysis pipeline that is more accessible to researchers lacking experience in image analysis, and uniquely, (*3*) the various components of the image and data analysis pipeline are dynamically interlinked. We have made VTEA freely available by digital download (Concise Methods).

The ability of VTEA to rapidly and automatically identify and quantify thousands of cells in 3D image volumes collected from the kidney enabled quantitative studies that would be impossible to conduct manually. For example, VTEA-based comparisons of volumes collected from different regions of the mouse kidney identified significant differences in the cell surface marker phenotype of resident immune cell between the cortex and outer stripe of the outer medulla. VTEA analyses were critical in identifying a depletion of immune cells in kidneys of THP knockout mice and showing that the depletion occurs predominantly in the inner stripe of the outer medulla, a point of biologic relevance, because this renal area is abundant in cells expressing THP. VTEA's ability to quantify cells in specific regions of the image volume was critical to detecting clustering of MHCII+ cells around glomeruli, an observation consistent with the hypothesis that intense immune surveillance occurs at the initial site of filtration.[4,9] We also showed how VTEA's ability to localize cells on the basis of quantitative criteria identified in scatterplots (gating) can be used as a discovery tool to identify subtle or unpredictable features, revealing the existence of a distinct subtype of proximal tubular epithelial cell population in the outer stripe expressing CD11C, a cell surface marker normally associated with myeloid cells.[2]

Although we have largely focused on the use of VTEA for characterizations of the local immune system *in situ*, this approach can easily be extended to the study of numerous other important biologic questions. These include the quantitative analysis of various structures in the kidney, such as glomerular size and distribution, tubular length and morphology, and the size of the interstitial space. VTEA's ability to efficiently characterize large volumes will facilitate detection and analysis of rare and stochastic events, such as apoptosis or other forms of cell death, with unprecedented precision and accuracy.

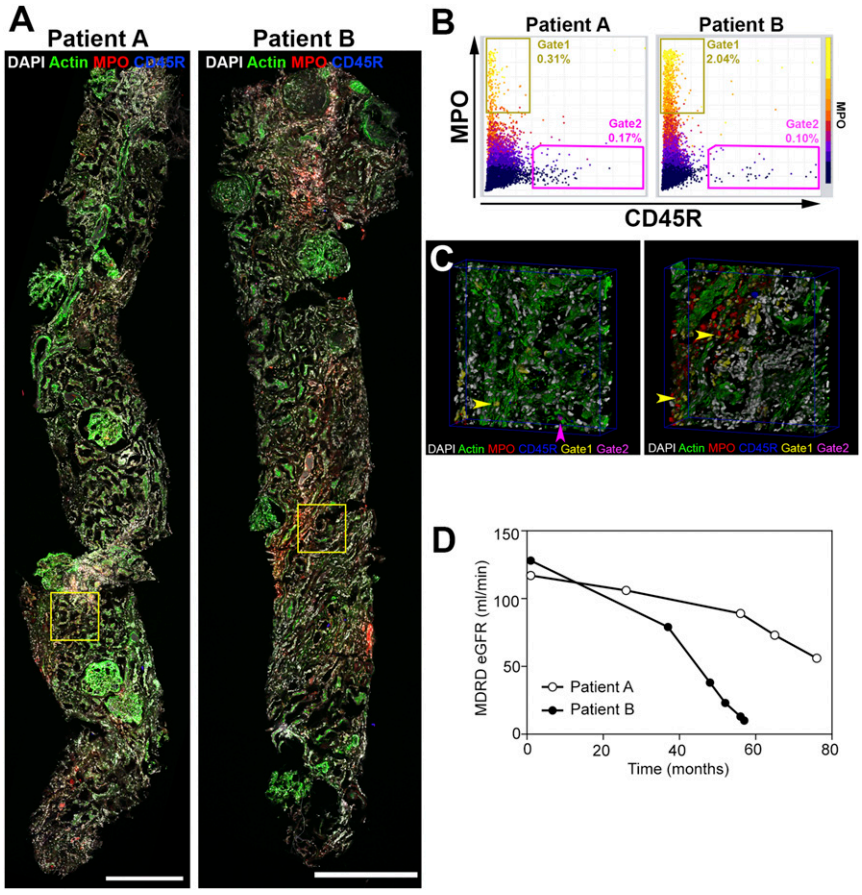

Figure 7. Using VTEA for large scale analysis of human kidney biopsy cores. VTEA can be applied to human biopsies to accurately quantitate infiltrating immune cells. Human kidney sections from biopsies taken from patients with diabetic nephropathy were fixed and stained for nuclei (white), F-actin (green), myeloperoxidase (MPO, red; neutrophil marker), and CD45R (blue; B lymphocyte marker). (A) Single optical sections of the stitched confocal image volumes obtained from two human biopsies. Scale bars, 0.5 mm. (B) Scatterplots of MPO versus CD45R immunofluorescence obtained from VTEA analysis of the image volumes shown in A. Gates drawn on each scatterplot were used to quantify the numbers of MPO+ and CD45R+ cells in each sample (gates 1 and 2, respectively). (C) 3D renderings of subregions of the biopsies shown in A (from the regions outlined in yellow). Nuclei of cells gated for expression of MPO or CD45R in B are indicated with yellow or magenta overlays. (D) Longitudinal measurements of Modification of Diet in Renal Disease eGFR for the patients from whom the biopsies were taken. VTEA results can be correlated to clinical patient data, such as progression of kidney disease. Patient B with rapid decline in kidney function had more infiltrating neutrophils.

We also show how VTEA could be used to study human kidney disease by supporting powerful 3D cytometry of human kidney core biopsies. The *in toto* aspect of the analysis will minimize sampling bias and ensure that rare events are not missed. The ability to quantify the abundance and distribution of various types of immune cells and detect their associations with particular tubules, blood vessels, or other specific morphologic parameters will add another layer of specificity in the analysis of these biopsies, which may provide additional insights into their interpretation. It is important to note that the biopsies shown in Figure 7 were stored frozen at −80°C for 3 years before analysis. The fact that these preserved specimens remain compatible with 3D tissue cytometry is particularly exciting, in that it suggests that the vast collection of frozen kidney biopsies stored by hospitals and academic health centers may represent an enormous untapped research resource, particularly when combined with longitudinal clinical data.

It should be pointed out that certain pathologies may alter the distribution and abundance of proteins used to identify specific cell types or structures.[16] Under these conditions, alternative markers would need to be identified and validated. For example, injured proximal tubules may lose some of their characteristic protein markers, but it is expected that they upregulate injury markers, such as KIM-1.[17,18]

The examples here show how VTEA-based 3D tissue cytometry provides the powerful capability to efficiently perform quantitative, multiparameter analyses of tissue specimens. In addition, performing large-scale 3D tissue cytometry on entire kidney core biopsies could profoundly increase the information

obtained from the vast repository of archival human tissue samples, providing a powerful new approach for investigating and understanding the pathogenesis of various forms of human kidney disease.

CONCISE METHODS

Institutional review board approval from Indiana University was obtained before using human nephrectomies and archived human biopsies. Animal studies were performed according to approved protocols from the Indiana University Institutional Animal Care and Use Committee. THP−/− mice and wild-type mice were used as described previously in multiple publications.[19,20]

Flow Cytometry

FC was performed as described previously on homogenized and digested kidneys from THP+/+ and THP−/− mice (n=4–5 per group[10]). A threshold for forward scatter was used to avoid cell debris and red blood cells, and the percentages reported were on live cells identified by exclusion of propidium iodide. A primary conjugated MHCII antibody (eBioscience) was used for labeling.

Tissue Sectioning and Immunofluorescence Staining

Immunofluorescence staining was done, as described previously, on 50-μm sections of 4% paraformaldehyde–fixed kidneys from mice and sectioned using a vibratome.[19–21] Human nephrectomy specimens were treated in the same manner. Human biopsy specimens were frozen in optimal cutting temperature compound after 12- to 24-hour protection in Michel solution after the biopsy procedures. After use in diagnostic pathology, the biopsy specimens were kept at −80°C, and they were subsequently biobanked according to an approved institutional review board protocol. The biopsy cores used in these experiments were from procedures performed in 2013. The frozen cores were sectioned at a thickness of 50 μm using a cryostat and immediately fixed using 4% paraformaldehyde. The following antibodies were used for mouse tissue against the following antigens: MHCII (14–5321–82; eBioscience) and CD11C (sc-2867C; Santa Cruz Biotechnology, Dallas, TX). For human tissue, we used the following antibodies: AQP1 (sc-9878; Santa Cruz Biotechnology), AQP2 (sc-28629; Santa Cruz Biotechnology), Myeloperoxidase (ab5690; Abcam), and CD45R (ab64100; Abcam). DAPI was used for staining nuclei. Oregon Green Phalloidin (Molecular Probes, Eugene, OR) was used for staining F-actin.

Image Acquisition

Image acquisition in three or four separate consecutive channels was performed using a Leica SP8 Confocal Microscope and/or an Olympus Fluoview Confocal Microscope System. Volume stacks spanning the whole thickness of the tissue were taken using a 20× NA 0.75 or 40× NA 1.3 objectives with 0.5- to 1.0-μm spacing. Large scale confocal imaging of overlapping volumes was performed with an automated stage and stitched using Leica LAS X software (Germany). 3D image rendering was done using Voxx v2.09d.[22]

3D Tissue Cytometry

The 3D tissue cytometry was performed on image volumes using VTEA, which was developed as a plugin for ImageJ/FIJI. The software is written entirely in Java and thus, runs on both Windows and Mac operating systems from within FIJI. It is written with dependencies on the FIJI framework as well as JXLayer (for Java 1.6 and earlier support, https://mvnrepository.com/artifact/org.swinglabs/jxlayer/3.0.4) and JFreeChart (http://www.jfree.org/jfreechart/). Source, licensing, and release version code are hosted on github (https://github.com/icbm-iupui/volumetric-tissue-exploration-analysis) and the FIJI update site (http://sites.imagej.net/ICBM-IUPUI/). VTEA was run in FIJI with ImageJ v1.51a and Java 1.8.0 on OSX running on a 1.2-GHz Intel Core m5 with 8 GB Random Access Memory (Figures 1–3 and 6, Supplemental Figures 1 and 4) or FIJI with ImageJ v1.49–1.51a and Java 1.7–1.8 on Windows 7 running on a pair of Xeon E5–2630v3 with 128 GB Random Access Memory (Figures 4, 5, and 7, Supplemental Figures 2 and 3).

The software allows volumetric cell identification on the basis of 3D nuclear segmentation using a blob-slice algorithm. 2D slices are segmented by intensity thresholding as entered by the user and subsequent 2D watershed splitting. Nuclei are constructed either on the basis of a nearest neighbor chain in 3D limited by a user-selected Euclidean distance and restricted to successive optical sections or with a 3D flood filling approach. Each nucleus identified is linked to the intensity of the associated labels in each channel in 3D by the dilation of the identified nucleus by a user-supplied distance. Identified cells were displayed on a scatterplot as individual points, which allowed gating, quantitation, and mapping of the objects on the image and automatic determination of the corresponding statistics.

Statistical Analyses

Values were displayed as means±SD. Statistics comparing two groups were done using a two-tailed paired t test at the 0.05 level of significance.

ACKNOWLEDGMENTS

Microscopy studies were conducted at the Indiana Center for Biological Microscopy. The authors acknowledge Dr. James Williams and Dr. Andrew Evan from the Department of Anatomy at Indiana University for assistance with kidney nephrectomy tissue.

This work was supported by a Veterans Affairs Merit Award (to T.M.E.-A.), National Institutes of Health (NIH)–National Institute of Diabetes and Digestive and Kidney Diseases (NIDDK) Program Project grant P01DK056788 (to T.M.E.-A.), and the Dialysis Clinic Inc. Research Fund (T.M.E.-A.). The Indiana Clinical and Translational Sciences Institute was funded, in part, by grant UL1 TR001108 from the NIH, National Center for Advancing Translational Sciences, Clinical and Translational Sciences Award. This work was also supported by NIH O'Brien Center for Advanced Renal Microscopic Analysis NIH-NIDDK grant P30DK079312.

DISCLOSURES

None.

REFERENCES

1. Kurts C, Panzer U, Anders HJ, Rees AJ: The immune system and kidney disease: Basic concepts and clinical implications. *Nat Rev Immunol* 13: 738–753, 2013
2. Nelson PJ, Rees AJ, Griffin MD, Hughes J, Kurts C, Duffield J: The renal mononuclear phagocytic system. *J Am Soc Nephrol* 23: 194–203, 2012
3. Li L, Okusa MD: Macrophages, dendritic cells, and kidney ischemia-reperfusion injury. *Semin Nephrol* 30: 268–277, 2010
4. Soos TJ, Sims TN, Barisoni L, Lin K, Littman DR, Dustin ML, Nelson PJ: CX3CR1+ interstitial dendritic cells form a contiguous network throughout the entire kidney. *Kidney Int* 70: 591–596, 2006
5. Li L, Huang L, Ye H, Song SP, Bajwa A, Lee SJ, Moser EK, Jaworska K, Kinsey GR, Day YJ, Linden J, Lobo PI, Rosin DL, Okusa MD: Dendritic cells tolerized with adenosine A_2AR agonist attenuate acute kidney injury. *J Clin Invest* 122: 3931–3942, 2012
6. Jang HR, Gandolfo MT, Ko GJ, Satpute SR, Racusen L, Rabb H: B cells limit repair after ischemic acute kidney injury. *J Am Soc Nephrol* 21: 654–665, 2010
7. Hull TD, Kamal AI, Boddu R, Bolisetty S, Guo L, Tisher CC, Rangarajan S, Chen B, Curtis LM, George JF, Agarwal A: Heme oxygenase-1 regulates myeloid cell trafficking in AKI. *J Am Soc Nephrol* 26: 2139–2151, 2015
8. Kawakami T, Lichtnekert J, Thompson LJ, Karna P, Bouabe H, Hohl TM, Heinecke JW, Ziegler SF, Nelson PJ, Duffield JS: Resident renal mononuclear phagocytes comprise five discrete populations with distinct phenotypes and functions. *J Immunol* 191: 3358–3372, 2013
9. Hato T, Winfree S, Kalakeche R, Dube S, Kumar R, Yoshimoto M, Plotkin Z, Dagher PC: The macrophage mediates the renoprotective effects of endotoxin preconditioning. *J Am Soc Nephrol* 26: 1347–1362, 2015
10. Micanovic R, Chitteti BR, Dagher PC, Srour EF, Khan S, Hato T, Lyle A, Tong Y, Wu XR, El-Achkar TM: Tamm-Horsfall protein regulates granulopoiesis and systemic neutrophil homeostasis. *J Am Soc Nephrol* 26: 2172–2182, 2015
11. Klingberg A, Hasenberg A, Ludwig-Portugall I, Medyukhina A, Männ L, Brenzel A, Engel DR, Figge MT, Kurts C, Gunzer M: Fully automated evaluation of total glomerular number and capillary tuft size in nephritic kidneys using lightsheet microscopy [published online ahead of print August 3, 2016]. *J Am Soc Nephrol* doi:10.1681/ASN.2016020232
12. Gerner MY, Kastenmuller W, Ifrim I, Kabat J, Germain RN: Histo-cytometry: A method for highly multiplex quantitative tissue imaging analysis applied to dendritic cell subset microanatomy in lymph nodes. *Immunity* 37: 364–376, 2012
13. Moreau HD, Lemaître F, Terriac E, Azar G, Piel M, Lennon-Dumenil AM, Bousso P: Dynamic in situ cytometry uncovers T cell receptor signaling during immunological synapses and kinapses in vivo. *Immunity* 37: 351–363, 2012
14. Liarski VM, Kaverina N, Chang A, Brandt D, Yanez D, Talasnik L, Carlesso G, Herbst R, Utset TO, Labno C, Peng Y, Jiang Y, Giger ML, Clark MR: Cell distance mapping identifies functional T follicular helper cells in inflamed human renal tissue. *Sci Transl Med* 6: 230ra46, 2014
15. Webster M, Witkin KL, Cohen-Fix O: Sizing up the nucleus: Nuclear shape, size and nuclear-envelope assembly. *J Cell Sci* 122: 1477–1486, 2009
16. Bonventre JV, Yang L: Cellular pathophysiology of ischemic acute kidney injury. *J Clin Invest* 121: 4210–4221, 2011
17. Han WK, Bailly V, Abichandani R, Thadhani R, Bonventre JV: Kidney Injury Molecule-1 (KIM-1): A novel biomarker for human renal proximal tubule injury. *Kidney Int* 62: 237–244, 2002
18. Takasu O, Gaut JP, Watanabe E, To K, Fagley RE, Sato B, Jarman S, Efimov IR, Janks DL, Srivastava A, Bhayani SB, Drewry A, Swanson PE, Hotchkiss RS: Mechanisms of cardiac and renal dysfunction in patients dying of sepsis. *Am J Respir Crit Care Med* 187: 509–517, 2013
19. El-Achkar TM, McCracken R, Rauchman M, Heitmeier MR, Al-Aly Z, Dagher PC, Wu XR: Tamm-Horsfall protein-deficient thick ascending limbs promote injury to neighboring S3 segments in an MIP-2-dependent mechanism. *Am J Physiol Renal Physiol* 300: F999–F1007, 2011
20. El-Achkar TM, Wu XR, Rauchman M, McCracken R, Kiefer S, Dagher PC: Tamm-Horsfall protein protects the kidney from ischemic injury by decreasing inflammation and altering TLR4 expression. *Am J Physiol Renal Physiol* 295: F534–F544, 2008
21. El-Achkar TM, McCracken R, Liu Y, Heitmeier MR, Bourgeois S, Ryerse J, Wu XR: Tamm-Horsfall protein translocates to the basolateral domain of thick ascending limbs, interstitium, and circulation during recovery from acute kidney injury. *Am J Physiol Renal Physiol* 304: F1066–F1075, 2013
22. Clendenon JL, Phillips CL, Sandoval RM, Fang S, Dunn KW: Voxx: A PC-based, near real-time volume rendering system for biological microscopy. *Am J Physiol Cell Physiol* 282: C213–C218, 2002

This article contains supplemental material online at http://jasn.asnjournals.org/lookup/suppl/doi:10.1681/ASN.2016091027/-/DCSupplemental.